Compact Dual-Band Dual-Polarized Stack Patch Antenna Array With Capacitive Feed for Fifth-Generation (5G) Applications

Behzad Ashrafi Nia and Franco De Flaviis

Abstract – In this article, a compact 4 × 4 dual-band dual-polarized antenna array with a wide bandwidth operating at the Ka band is presented. A stacked patch topology is used for dual-band operation, and feeding probes are used to excite the antenna array. Higher band elements have parasitic patches to achieve higher gain and increase the bandwidth. Moreover, a small metal ground on top of the common ground plane is designed for each element to suppress the coupling between the antenna elements and effectively improve the beam scanning range. The proposed antenna array with the size of 19 mm × 19 mm operates at the center frequencies of 28 GHz and 38 GHz, and the simulated results show that both wide bandwidth and stable gain were achieved. The 10 dB impedance bandwidths are 17.5% and 13.5% in the lower and higher bands, respectively. The realized gain is almost stable over the bandwidth and is around 16.45 dB and 17.28 dB for the lower and higher bands. Meanwhile, it has a relatively wide scanning angle, ranging from –45° to +45°, with stable gain and sidelobe level.

1. Introduction

Several frequency bands have been made available by the U.S. Federal Communications Commission for the incoming fifth-generation (5G) communications, including the Ka band at 28 GHz (27.5 GHz to 28.35 GHz), 37 GHz (37 GHz to 38.6 GHz), and 39 GHz (38.6 GHz to 40 GHz) [1]. Therefore, the design of a phased array antenna that can operate at multiple frequency bands is needed. This becomes more vital in multiple-input and multiple-output applications when there are several numbers of antennas. In this case, if the phased array antenna is designed with separated radiation apertures for different frequency bands, it occupies a large device area. Thus, designing a phased array antenna with a small footprint, wideband, high efficiency, low cost, and low mass to operate at multiple frequency bands will become a necessity. Moreover, it is more efficient to design a dual-polarized antenna to transmit and receive two orthogonal signals at the same time in the same aperture and be able to prevent polarization mismatch.

Manuscript received 8 December 2021.

Behzad Ashrafi Nia and Franco De Flaviis are with the Henry Samueli School of Engineering, University of California, Room 2233, Engineering Gateway, Irvine, California 92694, USA; e-mail: bashrafi@uci.edu, franco@uci.edu.

The type of design where multiple bands use the same aperture for radiation is called a shared aperture antenna [2, 3]. It has the advantage of a dual-polarization, multiband element combined design, and it is suitable for mobile platform applications [4–6]. Several shared aperture antennas with different radiation elements have been reported so far in the literature [7–12]. The first method of the shared aperture antenna is the dual-polarized antenna that operates at the same frequency band with orthogonal polarization. For this design, all the elements are usually symmetric, and the feed network is polarized orthogonally [13, 14]. The challenges appear when a dual-band antenna is needed, due to the different sizes of the antenna elements and spacing between them, especially, when the frequency ratio is large, which means that it occupies a large area.

The second is the inserting method in which the higher band elements are added into one lower band element, and they use the common aperture at the same time. In one of the previous designs, the lower band patch is penetrated to put the higher band elements inside it for dual-band shared aperture applications [2]. The result was 9.7% and 6.73% 10 dB impedance bandwidths for the Ku and X bands, respectively. In the other methodology, the radiating elements are interleaved at each band with the shared apertures [15]. In this work, the triband dual-polarized shared aperture array, where X-band elements and S-band elements were added in different parts of the L-band array, had results of 14.8%, 13.4%, and 16.8% bandwidth for the L band, S band, and X band, respectively. However, additional decoupling networks are usually required to enhance the feeding isolation for this configuration.

The third method in designing a shared aperture antenna is stacked technology, where the higher band element is placed above the lower band element [16, 17], and this method is used in this work. One of the issues of this method is high coupling between the lower and higher bands when operating in the dual-polarized array topology. The other challenge is sharing the same aperture for two separate arrays, operating at two widely separate frequencies without limiting the array scan capability. In this work, a compact dual-polarized dual-band antenna at the center frequencies of the 28 GHz and 38 GHz with a stacked technology, high isolation, simple structure, and wide scan ability, is introduced. The remainder of this article is arranged as follows: In Section 2, the antenna design of a single element and array structure is discussed, and then the simulation results will be presented for the single

element and the array. Finally, the conclusion is given in Section 3.

2. Design Concepts of the Antenna

The configuration of a dual-band dual-polarized (DBDP) antenna operating at the Ka band for 5G applications, is shown in Figure 1. For the future 5G application, the targeted bandwidth for the DBDP antenna is around 10% at center frequencies of 28 GHz and 38 GHz. The prospective 5G frequency bands are 26.5 GHz to 29.5 GHz and 37 to 40 GHz. This design consists of three layers. Substrates 1 and 2 are similar with the thickness of 468 μm and a relative permittivity of 3.14, with a loss of 0.002. The core layer is 200 μm thick, with a relative permittivity of 3.3 and a loss tangent of 0.003. As a result, the total thickness of the antenna is 1.136 mm. The stacked patch antenna configuration is implemented for the dual-band operation and low-profile antenna design.

2.1 Single Antenna Element

The radiating elements for the two bands are selected to be a patch. The low-band antenna (28 GHz) consists of a driven patch and two capacitive feeds to excite the antenna at two polarizations. The driven patch is placed on top of the core layer, as shown in Figure 1c, and fed by two perpendicular probes to achieve dual-polarization (Figures 1a and 1d). The high-band antenna (38 GHz) is placed inside substrate 2 and above the lower band (Figure 1b). Moreover, to improve the antenna bandwidth and gain, four parasitic rectangular elements are added in the same layer of the higher patch. These parasitic elements can add a new resonance near the primary patch resonance and, as a result, increase the bandwidth. Also, due to the inherent poor isolation of the capacitive feeding, these parasitic elements can improve isolation between the two orthogonal polarizations by reducing the amount of energy leaks to the adjacent element, if the antenna is used for dual-polarization application. If we consider the two ports on the patch as two separate antennas, the current on one antenna induces a current on the second antenna and leads to mutual coupling based on the reciprocity theorem. The parasitic element here neutralizes the first interelement coupling. In other words, the current that is directly induced on the second port by the first port is out of phase in comparison to the induced current by the parasitic element, and they will cancel each other out.

The dimensions of the patches and parasitic elements can be calculated as follows:

$$f_{L,H} = \frac{c}{2\mathrm{PL}_i\sqrt{\epsilon_i}} \; and \; f_{\mathrm{parasitic}} = \frac{c}{2\mathrm{Para\_L2}\sqrt{\epsilon_2}}, \; i = 1, 2 \tag{1}$$

where c is the speed of the light in the free space. $\mathrm{PL}_{1,2}$ and Para_L2 are the lengths of the driven low- and high-band patches and parasitic patch, respectively. Also, ε_1 and ε_2 are the effective dielectric constants for the two antennas. By tuning these lengths, the resonance frequency can be fixed at the desired bands that are 28 GHz and 38 GHz. The antenna is optimized by using the Ansys HFSS software (version 2021.1.0, Ansys 2021 R1, University of California Irvine), and the optimized parameters are given in the Table 1.

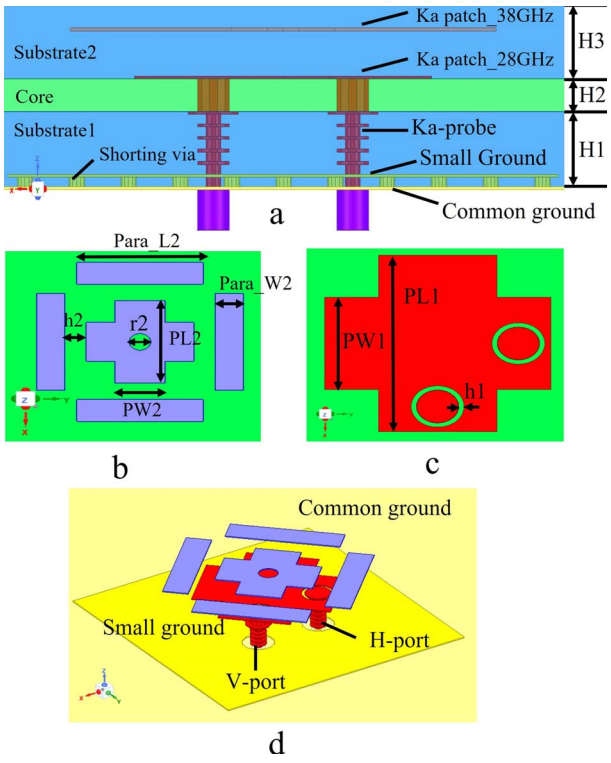

Figure 1. Layout of the proposed DBDP element. (a) Side view. (b) Top view of the higher band patch. (c) Top view of the lower band patch. (d) Perspective view of the lower band, higher band antenna, common, and small ground planes.

2.2 Probe Feeding and Individual Ground Plane

Figure 2 shows the side view of the feeding with more details, where the smaller patch is excited by two probes (vertical port and horizontal port). The height of the vias in the probe is 60 μm, and the radius of the vias and its pad are 60 μm and 125 μm, respectively. Figure 1 shows a compact antenna that is achieved by stacking patch antenna and parasitic elements. Another benefit of this design, as shown in Figure 1d, is that each antenna can be isolated from its adjacent elements by a small ground plane on top of the common ground plane. The distance between these two planes is 60 μm, and they are connected by multiple shorting vias. As a result, cross talk between components (caused by surface waves) decreases, and the scanning performance of the array will become better. However, the electrically long probing causes some mismatch due to excess inductance. To solve this problem, capacitive feeding is used by adding a gap between the probe and the lower band

Table 1. Parameters of the proposed antenna (mm)

H1	H2	H3	h1	h2	PL1
468	200	468	0.60	300	2135
PL2	PW1	PW2	Para_L2	Para_W2	r2
1500	1115	700	1765	365	300

patch. This gap forms the shunt capacitance to compensate for the inductance formed by a long probe from the ground plane to the substrate 2. As a result, with this type of feeding, it helps to use thicker substrates to achieve wider bandwidth.

2.3 Single-Element Performance

With the proper choice of dimensions for the lower and higher band patches, as well as for the parasitic elements and feeding, a large bandwidth is achieved at both frequency bands. In the final stage, the overall area of the antenna element is 3.8 mm × 3.8 mm. Figure 3a shows the reflection coefficient of the antenna. In these simulations, the DBDP antenna shows a −10 dB reflection coefficient with a wide bandwidth at both frequencies. This covers a 3.7 GHz bandwidth from 26.5 GHz to 30.2 GHz and a 4.9 GHz bandwidth from 35.2 GHz to 40.1 GHz for the lower and higher bands, respectively. This bandwidth covers the required frequency bands for the 5G applications in the Ka band. Moreover, as depicted in Figure 3a, the isolation between two feeds of the dual-polarized antenna is about 20 dB in the lower band and about 15 dB in the higher band.

The radiation performance of the single element in both frequency bands is simulated (Figures 3b and 3c). It can be observed that the antenna exhibits a stable radiation pattern over the bandwidth and with a peak realized gain of 6.5 dB and 7.2 dB for the lower and higher bands, as shown in Figure 3a, respectively. According to Figures 3b and 3c, the half-power beamwidth of a single element is 71° and 82° for the E plane and H plane and is 60° and 78° for the E plane and H plane for the lower and higher bands, respectively.

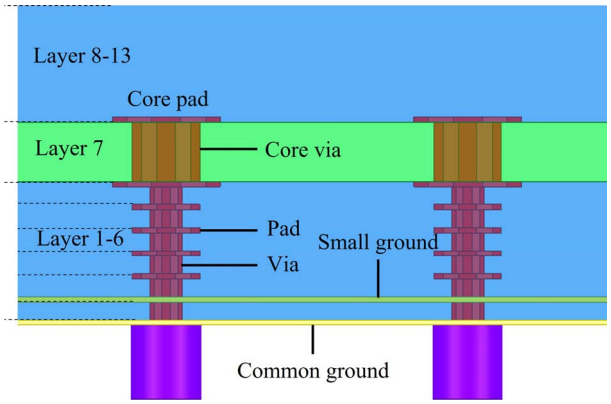

Figure 2. Stack up of the proposed DBDP element.

2.4 Antenna Array Performance

The designed single element in Section 2.3 allows making a 4 × 4 antenna patch array at the Ka band. The antenna should probably work over the whole band to cover the two desired bands that are 28 GHz and 38 GHz. The configuration of Figure 4 is used to implement the 4 × 4 array. As shown in the figure, the antenna elements are rotated 45° with respect to the substrate. This technique results in better isolation and decreases the coupling between adjacent antenna elements when used in an array configuration [18, 19].

To ensure that the phased array antenna has the maximum possible scanning angle without the phenomenon of grating lobes, the required element spacing d can be determined by using [20]:

$$d \leq \frac{\lambda}{1 + |\sin\theta|} \tag{2}$$

Here, λ is the operation wavelength at 28 GHz and 38 GHz, respectively. θ, the target scanning angle, is 45°, which is very challenging. Based on (2), the element spacing is set to be 4.4 mm due to the maximum element spacing for the lower band of 6.2 mm and 4.8 mm for the higher band. Therefore, the proposed dual-band and dual-polarized antenna array has total dimensions of 19 mm × 19 mm. The excitation for the array is the same as for the single element. The probe feeding will be designed on back of the common ground plane. This results in excellent isolation from the radiation pattern side. In this simulation, the antenna array is fed by a lump port with a uniform amplitude excitation.

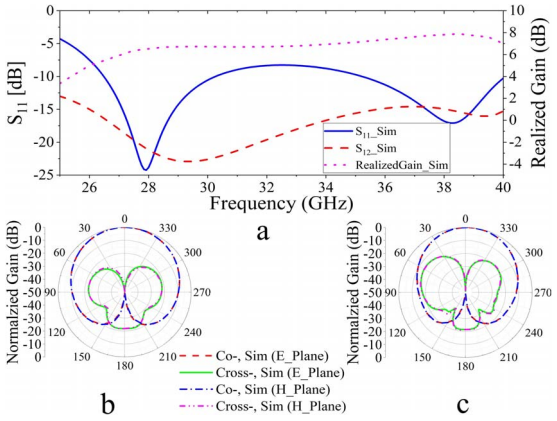

Figure 3. (a) S parameter and realized gain of the proposed single element. Normalized E_plane and H_plane radiation pattern at (b) 28.5 GHz and (c) 38.5 GHz.

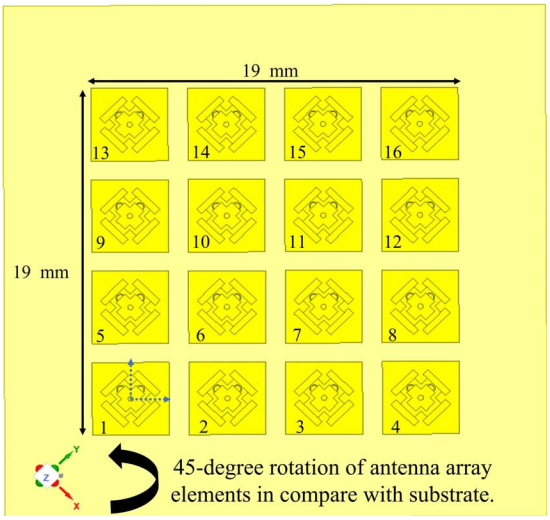

Figure 4. Configuration of the proposed antenna array.

The realized gain pattern for the array antenna at 28.5 GHz and 38.5 GHz for different scanning angles is shown in Figures 5a and 5b. This configuration shows a stable radiation pattern over different scanning angles from –45° to +45° for both frequency bands. The maximum realized gain is 16.46 dB and 17.28 dB for the lower band and higher band, respectively. Note that the maximum gain drops less than 3 dB while scanning in both azimuth and elevation directions for both desired bands. The sidelobes are simulated to be as low as 10 dB and 8 dB for the 45° scanning angle at the lower and higher bands, respectively.

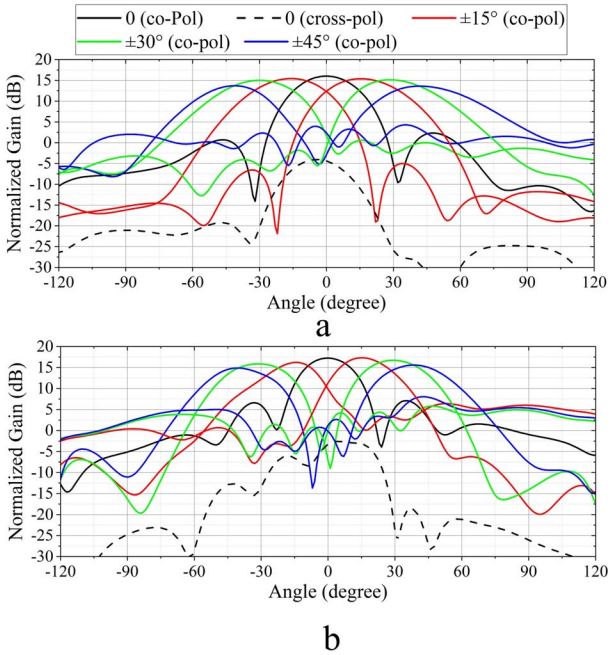

Figure 5. Simulated realized gain patterns in E plane for different scanning angles operating at (a) 28.5 GHz and (b) 38.5 GHz.

Table 2. Realized gain (dB) of the antenna array for different frequencies and scanning angles

Frequency (GHz)	0°	15°	30°	45°
27.5	16.45	16.1	15.6	13.8
28.5	16.46	16.5	15.5	13.8
29.5	16.49	16.6	15.3	13.9
37.5	17.28	15.4	16.5	14.8
38.5	16.8	16.2	16.8	15.5
39.5	17	16.01	16.3	15.4

It is also observed that the simulated crosspolar discriminations are about 21 dB in the broadside direction for both bands. More details of scanning angle and realized gain are shown in the Table 2 for six different operation frequencies and different scanning angles. The simulated S parameter of the three ports of the array antenna is shown in Figure 6. The simulated impedance bandwidth (active S parameter) ranges from 25.6 GHz to 30.5 GHz and 35.5 GHz to 40.5 GHz for the lower and higher bands, respectively. This bandwidth range corresponds to 17.5% and 13.5% bandwidth at 28 GHz and 38 GHz, respectively. It can be seen that in both E and H planes, the 3 dB beamwidth of the antenna array is 22° and 21° and 18° and 16° for the lower and higher bands, respectively. Therefore, based on these observations, this antenna array design can be recommended for 5G applications.

3. Conclusion and Future Work

In conclusion, our proposed antenna array demonstrates the following advantages: wide bandwidth, wide scanning angle, and a stable radiation pattern and gain over the Ka band. This makes it a great candidate for the next generation of 5G communication platforms. A compact DBDP antenna array is able to scan the wide angle from –45° to +45° with stable realized gain and an almost constant sidelobe level. It is also shown that the simulated impedance bandwidth is about 17.5% (from 25.6 GHz to 30.5 GHz) and 13.5% (from 35.5 GHz to 40.5 GHz) at center frequencies of 28 GHz and 38 GHz, respectively. The isolation between the two polarizations at the two bands is about 20 dB. The peak realized gain is 16.46 dB and 17.28 dB for the lower and higher bands as well.

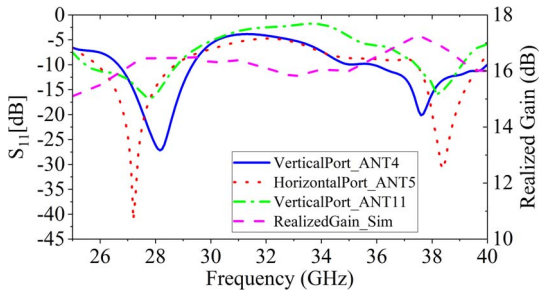

Figure 6. The active reflection coefficient for the 45° scanning angle (both polarization) and realized gain of the proposed antenna array.

4. References

1. U.S. Federal Communications Commission, "America's 5G Future," https://www.fcc.gov/5G (Accessed 23 November 2021).
2. J.-D. Zhang, W. Wu, and D.-G. Fang, "Dual-Band and Dual-Circularly Polarized Shared-Aperture Array Antennas With Single-Layer Substrate," *IEEE Transactions on Antennas and Propagation*, **64**, 1, January 2016, pp. 109-116.
3. Y. Wang and Z. Du, "Dual-Polarized Dual-Band Microstrip Antenna with Similar-Shaped Radiation Pattern," *IEEE Transactions on Antennas and Propagation*, **63**, 12, December 2015, pp. 5923-5928.
4. W. Hong, K. H. Baek, Y. Lee, Y. Kim, and S. T. Ko, "Study and Prototyping of Practically Large-Scale mmWave Antenna Systems for 5G Cellular Devices," *IEEE Communications Magazine*, **52**, 9, September 2014, pp. 63-69.
5. M. Stanley, Y. Huang, T. Loh, Q. Xu, H. Wang, et al., "A High Gain Steerable Millimeter-Wave Antenna Array for 5G Smartphone Applications," 11th European Conference on Antennas and Propagation, Paris, France, March 19–24, 2017, pp. 1311-1314.
6. M. Stanley, Y. Huang, H. Wang, H. Zhou, A. Al-Eiden, et al., "A Capacitive Coupled Patch Antenna Array with High Gain and Wide Coverage for 5G Smartphone Applications," *IEEE Access,* **6**, August 2018, pp. 41942-41954.
7. A. Boukarkar, X. Q. Lin, Y. Jiang, L. Y. Nie, P. Mei, et al., "A Miniaturized Extremely Close-Spaced Four-Element Dual-Band MIMO Antenna System With Polarization and Pattern Diversity," *IEEE Antennas and Wireless Propagation Letters*, **17**, 1, January 2018, pp. 134-137.
8. S. H. Yeung, A. García-Lampérez, T. K. Sarkar, and M. Salazar-Palma, "Thin and Compact Dual-Band Four-Element Broadside Patch Antenna Arrays," *IEEE Antennas and Wireless Propagation Letters,* **13**, 1, March 2014, pp. 567-570.
9. S. E. Valavan, D. Tran, A. G. Yarovoy, and A. G. Roederer, "Dual-Band Wide-Angle Scanning Planar Phased Array in X/Ku-Bands," *IEEE Transactions on Antennas and Propagation*, **62**, 5, May 2014, pp. 2514-2521.
10. G. Vetharatnam, C. B. Kuan, and C. H. Teik, "Combined Feed Network for a Shared-Aperture Dual-Band Dual-Polarized Array," *IEEE Antennas and Wireless Propagation Letters*, **4**, September 2005, pp. 297-299.
11. C.-X. Mao, S. Gao, Y. Wang, Q.-X. Chu, and X.-X. Yang, "Dual-Band Circularly Polarized Shared-Aperture Array for C-/X-Band Satellite Communications," *IEEE Transactions on Antennas and Propagation*, **65**, 10, Oct. 2017, pp. 5171-5178.
12. C.-X. Mao, S. Gao, Y. Wang, Q. Luo, and Q.-X. Chu, "A Shared-Aperture Dual-Band Dual-Polarized Filtering-Antenna-Array With Improved Frequency Response," *IEEE Transactions on. Antennas and Propagation*, **65**, 4, April 2017, pp. 1836-1844.
13. S. Chakrabarti, "Development of Shared Aperture Dual Polarized Microstrip Antenna at L-Band," *IEEE Transactions on Antennas and Propagation*, **59**, 1, January 2011, pp. 294-297.
14. Y. Shen, S.-G. Zhou, G.-L. Huang, and T.-H. Chio, "A Compact Dual Circularly Polarized Microstrip Patch Array With Interlaced Sequentially Rotated Feed," *IEEE Transactions on Antennas and Propagation*, **64**, 11, November 2016, pp. 4933-4936.
15. S. S. Zhong, Z. Sun, L. B. Kong, C. Gao, W. Wang, et al., "Tri-Band Dual-Polarization Shared-Aperture Microstrip Array for SAR Applications," *IEEE Transactions on Antennas and Propagation*, **60**, 9, September 2012, pp. 4157-4165.
16. P. Li, K. M. Luk, and K. L. Lau, "A Dual-Feed Dual-Band L-Probe Patch Antenna," *IEEE Transactions on Antennas and Propagation*, **53**, 7, July 2005, pp. 2321-2323.
17. Y. Wang and Z. Du, "Dual-Polarized Dual-Band Microstrip Antenna With Similar-Shaped Radiation Pattern," *IEEE Transactions on Antennas and Propagation*, **63**, 12, December 2015, pp. 5923-5928.
18. K. Woelder and J. Granholm, "Cross-Polarization and Sidelobe Suppression in Dual Linear Polarization Antenna Arrays," *IEEE Transactions on Antennas and Propagation*, **45**, 12, December 1997, pp. 1727-1740.
19. M. Mirmozafari and G. Zhang, "On Sidelobe Problem of Configured Array Antennas," *IEEE Transactions on Antennas and Propagation*, **66**, 7, July 2018, pp. 3475-3481.
20. R. J. Mailloux, *Phased Array Antenna Handbook*, 2nd Ed., Norwood, MA, Artech House, 2007.